

**High temperature catalysis: role of heterogeneous,
homogeneous, and radical chemistry**

To appear in:

“Catalysis”

Beller, Renken, van Santen (Eds.), Wiley-VCH, Weinheim 2011

Olaf Deutschmann²

Karlsruhe Institute of Technology (KIT)

Version 22.07.2010

*To whom correspondence should be addressed:

Prof. Dr. Olaf Deutschmann
Chair Chemical Technology at Karlsruhe Institute of Technology (KIT)
Engesserstr. 20, 76131 Karlsruhe, Germany

Tel.: +49 721 608-43138, Fax: -44805
Email: deutschmann@kit.edu

High temperature catalysis: role of heterogeneous, homogeneous, and radical chemistry

Olaf Deutschmann

Abstract

Selectivity and conversion in high-temperature catalysis is shown to often be the result of complex interactions of heterogeneous, homogeneous, and radical chemistry coupled with mass and heat transfer. The fundamental aspects as well as several applications of high-temperature catalysis are discussed in the light of these interactions. Applications cover synthesis of basic chemicals and hydrogen, and high-temperature fuel cells.

1. Introduction

This chapter focuses on heterogeneously catalyzed gas-phase reactions and their interaction with the surrounding flow field in high-temperature catalysis. Understanding and optimization of heterogeneous reactive systems require the knowledge of the physical and chemical processes on a molecular level. In particular, at short contact times and high temperatures, at which reactions occur on the catalyst and in the gas-phase, the interactions of transport and chemistry become important.

High-temperature catalysis is not a new concept; the Oswald process for the NO production by oxidation of ammonia over noble metal gauzes at temperatures above 1000°C and residence times of less than a micro second has been technically applied for decades; total oxidation of hydrogen and methane (catalytic combustion) over platinum catalysts were even used before Berzelius proposed the term “catalysis”. Recently, however, high-temperature catalysis has been extensively discussed again, in particular in the light of the synthesis of basic chemicals and hydrogen, and high-temperature fuel cells.

Catalytic partial oxidation (CPOX) of natural gas over noble metal catalysts at short contact times offers a promising route for the production of synthesis gas^[1, 2], olefins^[3, 4], and hydrogen. For instance, synthesis gas, also catalytically produced by steam and autothermal reforming, is needed in (gas-to-liquids) plants for synthetic fuels, which are currently under development. CPOX of gasoline, diesel, or alcohols to synthesis gas or hydrogen may soon play a significant role in mobile applications for reduction of pollutant emissions and auxiliary power units.

For any fuel other than hydrogen, catalytic reactions are likely to occur in the anode of a solid oxide fuel cell (SOFC) leading to a complex chemical composition at the anode-electrolyte interface^[5]. Primarily the products of the electrochemical reactions, H₂O and CO₂, drive the catalytic chemistry in the anode. For the application of hydrocarbon and alcohol containing fuels, the understanding of the catalytic kinetics is vital for the precise prediction of fuel utilization and performance^[6]. Coupling of the thermo catalytic reactions with the electrochemical processes and mass and heat transport in the cell will exemplarily be discussed for an anode-supported SOFC operated with methane containing fuels and a Ni/YSZ anode structure.

2. Fundamentals

Catalytic reactors are generally characterized by the complex interaction of various physical and chemical processes. Monolithic reactors can serve as example, in which partial oxidation and reforming of hydrocarbons, combustion of natural gas, and the reduction of pollutant emissions from automobiles are frequently carried out. Figure 1 illustrates the physics and chemistry in a catalytic combustion monolith that glows at a temperature of about 1300 K due to the exothermic oxidation reactions. In each channel of the monolith, the transport of momentum, energy, and chemical species occurs not only in flow (axial) direction, but also in radial direction. The reactants diffuse to the inner channel wall, which is coated with the catalytic material, where the gaseous species adsorb and react on the surface. The products and intermediates desorb and diffuse back into the bulk flow. Due to the high temperatures, the chemical species may also react homogeneously in the gas phase. In catalytic reactors, the catalyst material is often dispersed in porous structures like washcoats or pellets. Mass transport in the fluid phase and chemical reactions are then superimposed by diffusion of the species to the active catalytic centers in the pores.

The temperature distribution depends on the interaction of heat convection and conduction in the fluid, heat release due to chemical reactions, heat transport in the solid material, and thermal radiation. If the feed conditions vary in time and space and/or heat transfer occurs between the reactor and the ambience, a non-uniform temperature distribution over the entire monolith will result, and the behavior will differ from channel to channel^[7].

Today, the challenge in catalysis is not only the development of new catalysts to synthesize a desired product, but also the understanding of the interaction of the catalyst with the surrounding reactive flow field. Sometimes, the exploitation of these interactions can lead to the desired product selectivity and yield. A detailed introduction into fluid dynamics and transport phenomena can be found in ^[8-12], and into the coupling with heterogeneous reactions in ^[12, 13].

2. 1. Heterogeneous reaction mechanisms

The development of a reliable surface reaction mechanism is a complex process. A tentative reaction mechanism can be proposed based on experimental surface science studies, on analogy to gas-phase kinetics and organo-metallic compounds, and on theoretical studies, increasingly including DFT calculations. This mechanism should include all possible paths for the formation of the chemical species under consideration in order to be “elementary-like” and thus applicable over a wide range of conditions. The mechanism idea then needs to be evaluated by numerous experimentally derived data, which are compared with theoretical predictions based on the mechanism. Here, the simulations of the laboratory reactors require appropriate models for all significant processes in order to evaluate the intrinsic kinetics. Sensitivity analysis leads to the crucial steps in the mechanism, for which refined kinetic experiments and data may be needed.

Since the early nineties, many groups have developed surface reaction mechanisms for high-temperature catalysis, following this concept, which has been adapted from modeling homogeneous gas-phase reactions in particular in the fields of combustion^[10] and pyrolysis^[14] of hydrocarbons. Consequently, this concept becomes handy when high-

temperature processes in catalysis are considered, in particular the radical interactions between the solid phase (catalyst) and the surrounding gas-phase (fluid flow).

In this concept, the surface reaction rate is related to the size of the computational cell in the flow field simulation assuming that the local state of the active surface can be represented by mean values for this cell. Hence, this model assumes randomly distributed adsorbates. The state of the catalytic surface is described by the temperature T and a set of surface coverages θ_i . The surface temperature and the coverages depend on time and the macroscopic position in the reactor, but are averaged over microscopic local fluctuations. Under those assumptions the molar net production rate \dot{s}_i of a chemical species on the catalyst is given as

$$\dot{s}_i = \sum_{k=1}^{K_s} \nu_{ik} k_{f_k} \prod_{j=1}^{N_g+N_s+N_b} c_j^{\nu_{jk}}. \quad (1)$$

Here, K_s is the number of surface reactions, c_i are the species concentrations, which are given, e.g., in mol m⁻² for the N_s adsorbed species and in, e.g., mol m⁻³ for the N_g and N_b gaseous and bulk species. According to the relation

$$\Theta_i = c_i \sigma_i \Gamma^{-1}, \quad (2)$$

where Γ is surface site density with a coordination number σ_i describing the number of surface sites which are covered by the adsorbed species, the variations of surface coverages follow

$$\frac{\partial \Theta_i}{\partial t} = \frac{\dot{s}_i \sigma_i}{\Gamma}. \quad (3)$$

Since the reactor temperature and concentrations of gaseous species depend on the local position in the reactor, the set of surface coverages also varies with position. However, no lateral interaction of the surface species between different locations on the catalytic surface is modeled. This assumption is justified by the fact that the computational cells in reactor simulations are usually much larger than the range of lateral interactions of the surface processes.

Since the binding states of adsorption of all species vary with the surface coverage, the expression for the rate coefficient k_{f_k} is commonly extended by two additional parameters, μ_{i_k} and ε_{i_k} [12, 15].

$$k_{f_k} = A_k T^{\beta_k} \exp\left[\frac{-E_{a_k}}{RT}\right] \prod_{i=1}^{N_s} \Theta_i^{\mu_{i_k}} \exp\left[\frac{\varepsilon_{i_k} \Theta_i}{RT}\right] \quad (4)$$

A crucial issue with many of the surface mechanisms published is thermodynamic consistency^[13]. Lately, optimization procedures enforcing overall thermodynamic consistency have been applied to overcome this problem^[16].

In particular oxidation reactions, in which radical interactions play a very significant role, have been modeled extensively using this approach such as oxidation of hydrogen ^[17-23], CO ^[24-26], and methane ^[27-32] and ethane ^[4, 33-35] over Pt, formation of synthesis gas over Rh ^[32, 36]. Lately, mechanisms have been established for more complex reaction systems, for instance, three-way catalysts ^[37] or Chemical Vapor Deposition (CVD) reactors for the formation of diamond ^[38, 39], silica ^[40], and nanotubes ^[41]. In most of these reactions, adsorption and desorption of radicals is included and these steps are significant not only for the heterogeneous reaction but also for homogeneous conversion in the surrounding fluid. In most cases, the catalyst acts as sink for radicals produced in the gas-phase, and hence radical adsorption inhibits gas-phase reactions as exemplarily discussed below for oxy-dehydrogenation of alkanes by high-temperature catalysis.

2.2 Homogeneous reactions

In many catalytic reactors, the reactions do not exclusively occur on the catalyst surface but also in the fluid flow. In some reactors even the desired products are mainly produced in the gas phase, for instance in the oxidative dehydrogenation of paraffins to olefins over noble metals at short contact times and high temperature as discussed below ^[4, 35, 42-47]. Such cases are dominated by the interaction between gas-phase and surface kinetics and transport. Therefore, any reactor simulation needs to include an appropriate model for the homogeneous kinetics along with the flow models. With ν'_{ik} , ν''_{ik} being the stoichiometric coefficients and an Arrhenius-like rate expression, the chemical source term of homogeneous reactions can be expressed by

$$R_i^{\text{hom}} = M_i \sum_{k=1}^{K_g} (\nu''_{ik} - \nu'_{ik}) A_k T^{\beta_k} \exp\left[\frac{-E_{a_k}}{RT}\right] \prod_{j=1}^{N_g} \left(\frac{Y_j \rho}{M_j}\right)^{a_{jk}} \quad (5)$$

Here, A_k is the pre-exponential factor, β_k is the temperature exponent, E_{a_k} is the activation energy, and a_{jk} is the order of reaction k related to the concentration of species j . Various reliable sets of elementary reactions are available for modeling homogeneous gas phase reactions, for instance for total ^[10] and partial oxidation, and pyrolysis of hydrocarbons. The advantage of the application of elementary reactions is that the reaction orders a_{jk} in Eq. (5) equal the stoichiometric coefficients ν'_{jk} .

2.3 Coupling of chemistry and mass and heat transport

The chemical processes at the surface can be coupled with the surrounding flow field by boundary conditions for the species-continuity equations at the gas-surface interface ^[12, 15]:

$$\vec{n}(\vec{j}_i + \rho \vec{v}_{\text{Stef}} Y_i) = R_i^{\text{het}} \quad (6)$$

Here \vec{n} is the outward-pointing unit vector normal to the surface, \vec{j}_i is the diffusion mass flux of species i and R_i^{het} is the heterogeneous surface reaction rate, which is given per unit geometric surface area, corresponding to the reactor geometry, in $\text{kg m}^{-2} \text{s}^{-1}$. The Stefan velocity \vec{v}_{Stef} occurs at the surface if there is a net mass flux between the surface and the gas phase^[27, 48]. The calculation of R_i^{het} requires the knowledge of the amount of catalytically active surface area in relation to the geometric surface area, here denoted by $F_{\text{cat/geo}}$, at the gas-surface interface:

$$R_i^{\text{het}} = \eta F_{\text{cat/geo}} M_i \dot{s}_i \quad (7)$$

Here, \dot{s}_i is the molar net production rate of gas phase species i , given in $\text{mol m}^{-2} \text{s}^{-1}$; the area now refers to the actual catalytically active surface area. $F_{\text{cat/geo}}$ can be determined experimentally, e.g. by chemisorption measurements. The effect of internal mass transfer resistance for catalyst dispersed in a porous media is included by the effectiveness factor η ^[11, 49]. For more detailed models for transport in porous media it is referred to literature^[50, 51].

Modeling the flow field in laminar and turbulent flows is discussed in many textbooks^[8, 10] and review articles we refer to. Even though the implementation of Eqs. (5-7) in those fluid flow models is straight forward, an additional highly nonlinear coupling is introduced into the governing equations describing the flow field (leading to considerable computational efforts. The nonlinearity, the large number of chemical species, and the fact that chemical reactions exhibit a large range of time scales, in particular when radicals are involved, make the solution of those equation systems challenging. In particular for turbulent flows, but sometimes even for laminar flows, the solution of the system is too CPU time-consuming with current numerical algorithms and computer capacities. This calls for the application of reduction algorithms for large reaction mechanisms, for instance by the extraction of the intrinsic low dimensional manifolds of trajectories in chemical space^[52], which can be applied for heterogeneous reactions^[53]. Another approach is to use “as little chemistry as necessary”. In these so-called adaptive chemistry methods, the construction of the reaction mechanism includes only steps relevant for the application studied^[54].

2.4. Monolithic catalysts

As an example of a modeling a high-temperature catalyst, catalytically coated monolithic structures as given in Fig. 1 are discussed. An efficient approach, which still includes all fundamental aspects, is often used for modeling catalytic monoliths, which is based on the combination of simulations of a representative number of channels with the simulation of the temperature profiles of the solid structure treating the latter one as continuum^[55, 56]. This approach is the basis for the computer code DETCHEM^{MONOLITH}^[57], which has been applied to model the transient behavior of catalytic monoliths. The code combines a transient three-dimensional simulation of a catalytic monolith with a 2D model of the single-channel flow field based on the boundary layer approximation. It uses detailed models for homogeneous gas-phase chemistry, heterogeneous surface chemistry, and contains a model for the description of pore diffusion in washcoats.

The numerical procedure as sketched in Fig. 2 is based on the following ideas: The residence time of the reactive gas in the monolith channels is much smaller than the unsteadiness of the inlet conditions and the thermal response of the solid monolith structure. Under these assumptions, the time scales of the channel flow are decoupled from the temporal temperature variations of the solid, and the following procedure can be applied: A transient multi-dimensional heat balance is solved for the monolithic structure including the thermal insulation and reactor walls, which are treated as porous continuum. This simulation of the heat balance provides the temperature profiles along the channel walls. At each time step the reactive flow through a representative number of single channels is simulated including detailed transport and chemistry models. These single-channel simulations also calculate the heat flux from the fluid flow to the channel wall due to convective and conductive heat transport in the gaseous flow and heat released by chemical reactions. Thus, at each time step, the single-channel simulations provide the source terms for the heat balance of the monolith structure while the simulation of the heat balance provides the boundary condition (wall temperature) for the single-channel simulations. At each time step, the inlet conditions may vary. This very efficient iterative procedure enables a transient simulation of the entire monolith without sacrificing the details of the transport and chemistry models, as long as the prerequisites for the time scales remain valid. Furthermore, reactors with alternating channel properties such as flow directions, catalyst materials, and loadings can be treated.

2.5 Experimental evaluation of models describing radical interactions

The coupling of several complex models introduces a large number of parameters into the simulations. Hence, agreement between predicted and experimentally observed overall conversion and selectivity alone is not sufficient to evaluate individual sub models. Time and locally resolved profiles provide a more stringent test for model evaluation. Useful data arise from the experimental resolution of local velocity profiles by laser Doppler anemometry/velocimetry (LDA, LDV)^[58, 59] and of spatial and temporal species profiles by in situ, non-invasive methods such as Raman and laser induced fluorescence (LIF) spectroscopy. For instance, an optically accessible catalytic channel reactor can be used to evaluate models for heterogeneous and homogeneous chemistry as well as transport by the simultaneous detection of stable species by Raman measurements and OH radicals by Planar laser-induced fluorescence (PLIF)^[60, 61].

2.6 Mathematical optimization of reactor conditions and catalyst loading

In a chemical reactor, the initial and boundary conditions can be used to optimize the performance of the reactor, i.e., maximize the conversion, the selectivity or the yield of certain product species. In particular, at the inlet of the catalytic monolith, the mass or molar fractions of the species, the initial velocity, or the initial temperature can be controlled to optimize one product composition. Furthermore, it may be possible to control the temperature profile $T_{\text{wall}}(z)$ at the channel wall, and vary the loading with catalyst along the channel, i.e., $F_{\text{cat/geo}}(z)$. Moreover, the length of the catalytic monolith z_{max} can be optimized. Recently, algorithms have been established to not only optimize those control parameters but also to be applied to achieve a better understanding of the interactions between heterogeneous and homogeneous chemical reactions in catalytic reactors^[62-64]. Radical interaction may play a decisive role as shown in the example given below.

3. Applications

3.1. Turbulent flow through channels with radical interactions

Mantzaras et al.^[65] applied the k - ε model, a presumed (Gaussian) probability density function for gaseous reactions, and a laminar-like closure for surface reactions to study turbulent catalytically stabilized combustion of lean hydrogen-air mixtures in plane platinum-coated channels. Here the two-dimensional OH profiles as shown in Fig. 3 reveal the interaction of gas-phase and surface chemistry; depending on the position in the reactor, the profiles as function of distance from the catalyst vary significantly. They also examined different low-Reynolds number near-wall turbulence models and compared the numerically predicted results with data derived from planar laser-induced fluorescence measurements of OH radicals, Raman measurements of major species and laser doppler velocimetry measurements of local velocities and turbulence^[66]. They found that discrepancies between predictions and measurements are ascribed to the capacity of the various turbulence models to capture the strong flow laminarization induced by the heat transfer from the hot catalytic surfaces.

3.2. Synthesis gas from natural gas by high-temperature catalysis

Another class of tube-like reactors is the monolith or honeycomb structure, which consists of numerous passageways with diameters reaching from a tenth of a millimeter to few millimeters. The flow field in the thin channels of this reactor type is usually laminar. The catalytic material is mostly dispersed in a washcoat on the inner channel wall. Monolith channels are manufactured with various cross-sectional shapes, e.g., circular, hexagonal, square or sinusoidal. In the next sections, the configuration of catalytic monolithic reactors will be used to discuss the interaction of gas-phase and surface chemistry in high-temperature catalysis.

The high-temperature catalytic partial oxidation (CPO) of methane over Rh based catalysts in short contact time (milliseconds) reactors has been intensively studied, because it offers a promising route to convert natural gas into synthesis gas (syngas, H_2 and CO), which can subsequently be converted to higher alkanes or methanol or be used in fuel cells^[1, 67, 68]. The indirect route for syngas formation has meanwhile been accepted; at the catalyst entrance total

oxidation occurs to form steam as long as oxygen is available at the surface, then methane is steam-reformed to hydrogen. Basically no dry reforming occurs and the surface acts as sink for radicals inhibiting significant gas-phase reactions at pressures below 10 bar^[69]. Also the transient behavior during light-off of the reaction has been revealed. Exemplarily, Figure 4 shows the time-resolved temperature and species profiles in a single channel of a catalytic monolith for partial oxidation of methane for the production of synthesis gas and the temperature distribution of the solid structure during light-off^[36].

Since natural gas contains higher alkanes and other minor components besides methane, conversion and selectivity can be influenced by those other components. Consequently, conversion of methane in steam reforming of pure methane and in steam reforming of natural gas (North Sea H) differ as shown in Figure 5. Here, fuel/steam mixtures, molar steam to carbon ratio of 2.5 and 4, diluted by 75% Ar, 10000 h⁻¹ space velocity, were fed into a furnace containing a Rh coated honeycomb catalyst^[70].

3.2. Olefin production by high-temperature oxidative dehydrogenation of alkanes

While gas-phase reactions are not significant in CPOX of methane at atmospheric pressure, CPOX of ethane to ethylene over platinum coated catalysts at short contact times^[71, 72] is characterized by complex interactions of homogeneous gas-phase and heterogeneous surface reactions^[4, 44, 73]. The principal picture of the reaction process is shown in Fig. 6. At the catalyst entrance oxygen is completely consumed at the surface within 1 mm primarily producing CO₂ and H₂O. This total combustion of ethane leads to a rapid temperature increase from RT to 1000°C. The high temperature drives the pyrolysis of ethane in the gas-phase. After a decade of discussions on the reaction pathways, most studies today conclude that most of the ethylene (desired product) is actually homogeneously produced in the gas-phase. Further downstream, additionally, reforming and shift reactions occur.

Based on the molecular understanding of interaction of gas-phase and surface chemistry in oxy-dehydrogenation of ethane over Pt^[4], Minh et al. ^[62] used a recently developed optimization code to find the optimal Pt catalyst loading on along the flow direction in a Pt/Al₂O₃ coated honeycomb catalyst. The gas-phase mechanism used consists of 25 reactive species (mainly C1 and C2 species) involved in 131 reversible reactions and one irreversible reaction, and the surface reaction mechanism consists of another 82 elementary-step like reactions involving another 19 surface species.^[4] This mechanism was later also used to study on-line catalyst addition effects^[73]. The Pt coated monolith had a diameter of 18 mm and a length of 10 mm. Each channel has a diameter of 0.5 mm. The monolith is fed with ethane/oxygen/nitrogen mixture of varying C/O ratio at 5 standard liters per minute leading to a residence time of few milliseconds.

Formulation of an Optimal Control Problem: The initial and boundary conditions can be used to optimize the performance of the reactor, i.e., maximize the conversion, the selectivity or the yield of certain product species. In particular, at the inlet of the catalytic monolith, the mass or molar fractions of the species, the initial velocity, or the initial temperature can be controlled to optimize one product composition. Furthermore, it may be possible to control the temperature profile $T_{\text{wall}}(z)$ along the channel wall, and vary the loading with catalyst along the channel, i.e., $F_{\text{cat}/\text{geo}}(z)$. Moreover, the length of the catalytic monolith z_{max} can be optimized. Here, the objective function to

be maximized is the mass fraction of ethylene at the outlet of the channel. The control considered here is the catalyst loading, expressed, which is a function of the axial coordinate z . For practical reasons, there are often equality and inequality constraints on the control and state variables, such as an upper and lower bounds for the catalyst loading and the (trivial) fact that the sum of all mass fractions must be one.

In the case considered, the inlet gas temperature is $T_{\text{gas}} = 600 \text{ K}$, and the wall temperature $T_{\text{wall}}(z)$ is kept fixed at 1000 K. As constraint the $F_{\text{cat/geo}}(z)$ is required to be between 0, i.e., no catalyst, and 100, i.e., highly loaded. The optimization was started with a constant $F_{\text{cat/geo}}(z)$ profile of 20.0 leading to an objective value of 0.06. In the optimal solution the objective value is 0.19. Figure 7 shows the standard and optimal profiles of $F_{\text{cat/geo}}(z)$ and average mass fraction profiles of ethylene. Figure 8 reveals the mass fraction profiles of ethane and ethylene with the optimal profile of $F_{\text{cat/geo}}(z)$. Platinum is a very efficient catalyst for the oxidation of ethane. In the first two mm of the catalyst, oxygen is almost completely consumed by surface reactions (catalytic oxidation of ethane) leading to the total oxidation products CO_2 and H_2O , ethylene, and some CO. Ethylene however is substantially produced in the gas-phase as well. However, the conversion in the gas-phase only occurs if a sufficiently large radical pool is build up, which takes a certain time/distance (so-called ignition delay time). Furthermore, some of the ethylene formed by surface reactions adsorb on the surface as well, where in the region around 2 mm mainly reforming reactions occur but the total reaction rate is much smaller than in the first mm of the catalyst where oxygen was still available. Since the production of ethylene by gas-phase reactions really takes-off further downstream (most of the ethylene is produced in the gas-phase) due to the radicals available there and due to the fact that the surface is relatively inactive in the region around 2 mm, a plateau appears in that region around 2 mm (Fig. 7) due to the competition between ethylene production in the gas-phase and (partial) oxidation on the surface, both at relatively low rates. The optimization of the catalyst loading proposes a very low loading in this region, because here the catalyst does not only oxidize ethylene but also adsorbs radicals from the gas-phase, which are needed to initiate ethylene formation in the gas-phase. The optimization proposes relatively low catalyst loading in the very active initial catalyst section, which can be understood as follows: Within the first mm of the catalyst, where oxygen is available, the process is limited by mass-transfer of ethane and even more of oxygen to the surface. Here, primarily, oxidation of ethane occurs at a very high rate, the catalyst is very active. Consequently, catalyst is needed here but not at a high loading; this effect has also been observed in several experiments.

The hydrocarbon/oxygen (C/O) ratio can easily be used to tune the product selectivity in CPOX of alkanes. The group of L.D. Schmidt has studied a variety of fuels and basically found the same trend as shown in Fig. 6 for CPOX of n-decane at millisecond contact times over Rh catalysts^[46]. At low C/O ratio, synthesis gas is the primary product; actually its maximum is reached close to the point where the reaction switches to total combustion, a flame is often formed in that transition region. With increasing C/O ratio, more and more olefins are formed, primarily α -olefins, but at higher C/O ratio a larger variety of other olefins as well, and eventually acetylene, benzene, and PAH are formed at very low oxygen content. Coking of the catalyst and formation of soot in the gas-phase quickly becomes a technical problem. Those studies over noble metal based catalysts and at millisecond contact times were recently extended to CPOX of biodiesel^[74]. Also, autothermal reforming of ethanol was realized at short contact times and high temperatures in a two-stage reactor^[75, 76]. A Rh – ceria catalyst on alumina foams/spheres served as

first stage for reforming with some oxygen addition. The second reactor stage consists of Pt – ceria on alumina spheres to accelerate the water-gas shift reaction for maximizing the hydrogen yield.

3.3. Hydrogen production from logistic fuels by high-temperature catalysis

The production of hydrogen and synthesis gas (syngas, H₂ and CO) from logistic fuels such as gasoline, diesel, and kerosene by catalytic partial oxidation (CPOX) and steam reforming (SR) is currently in the focus of both academic and industrial research. In contrast to the complex and costly supply of compressed and stored hydrogen for mobile fuel cell application, CPOX of liquid fuels allows production and utilization of hydrogen through existing routes, which, in particular, is of interest for on-board applications. At operating temperatures around 1000 K and higher, conversion of the fuel may not only occur on the solid catalyst but also in the gas-phase. Heterogeneous and homogeneous reactions in CPOX of hydrocarbons are coupled not only by adsorption and desorption of fuel and oxygen molecules and the products, respectively, but also by adsorption and desorption of intermediates and radicals. Therefore, mass transport of radicals and intermediates from/to the gaseous bulk phase and the catalytically active channel wall, mainly by radial diffusion in the small channels of the monolith being on the order of a quarter to one millimeter, is crucial for the interaction of heterogeneous and homogeneous reactions in CPOX reactors. Hartmann et al., for instance, studied the catalytic partial oxidation of iso-octane over rhodium/alumina coated honeycomb monolith serving as gasoline surrogate^[77]. Very high hydrogen and carbon monoxide selectivity were found at stoichiometric conditions (C/O = 1), while at lean conditions more total oxidation occurs. At rich conditions (C/O > 1), homogeneous chemical conversion in the gas-phase is responsible for the formation of by-products such as olefins shown in Fig. 10 that also have the potential for coke formation, which was observed experimentally and numerically. This study also revealed that the chemical models applied – even though the most detailed ones available (857 gas-phase and 17 adsorbed species in over 7000 elementary reactions) were used – need further improvement.

Nevertheless, this combined modeling and experimental study revealed the role of surface, gas-phase, and radical chemistry in high-temperature oxidative catalytic conversion of larger hydrocarbons. From Figures 11, it can clearly be concluded that the major products (syngas) are produced in the entrance region of the catalyst on the catalytic surface; radial concentration profiles are caused by a mass-transfer limited process. As soon as the oxygen is consumed on the catalytic surface – similar to CPOX of natural gas – hydrogen formation increases due to steam reforming, the major products are formed within few millimeters. At rich conditions (C/O>1.0) a second process, now in the gas-phase, begins in the downstream part as shown in Fig. 12. The number of radicals in the gas-phase is sufficiently large to initiate gas-phase pyrolysis of the remaining fuel and formation of coke-precursors such as ethylene and propylene. In the experiment, the downstream part of the catalyst is coked-up, here the Rh surface cannot act as sink for radical.

3.4. High-temperature catalysis in Solid Oxide Fuel Cells

In the recent past solid oxide fuel cells (SOFC) have attracted considerable attention due to its potential to convert chemical energy into electrical energy at high efficiencies. SOFCs are also called high-temperature fuel cells, because they are operated at temperature of approximately 800°C, and, therefore (no CO poisoning) they have the

potential of a direct use of hydrocarbons and alcohols as fuels^[78]. A sketch of the major processes in an anode-supported solid oxide fuel cells operated with hydrocarbons is shown in Fig. 13^[5]. The anode contains an electron conductor, e.g. nickel, and an ion conducting material, e.g. yttria stabilized zirconia (YSZ). High-temperature catalytic reactions proceed on the Ni surface; steam as major product of the electrochemical reaction drives the endothermic reforming of the incoming fuel producing hydrogen, that eventually takes part in the charge transfer reaction.

Understanding the performance of a SOFC requires the understanding of the interaction of electro catalysis, electric fields, current density, thermo-catalytic reactions on the metal surface, potential homogeneous reactions in the gas phase (in particular for fuels containing liquid hydrocarbons), mass and heat transport in the fuel and air channels and inside the porous membrane electrode assembly (MEA). Several groups^[5, 79] applied the following approach for their the analysis of temperature, species concentrations, and current density profiles as well as the efficiency and power density of a planar solid oxide fuel cell at direct internal reforming conditions: The heterogeneous chemistry model of the catalytic reactions in the anode structure uses a multi-step reaction mechanism for the steam reforming of methane on Ni based catalysts^[6]. The porous media transport is modeled using the Dusty Gas Model, and electrochemistry is modeled using a modified Butler-Volmer setting assuming hydrogen as the only electrochemically active species^[80]. The channel flows are usually model by plug flow equations.

High-temperature catalysis in SOFCs will now exemplarily be discussed for an anode-supported SOFC operated with methane containing fuels and a Ni/YSZ anode structure. The simulation reveals the species concentrations in the fuel channel and the porous anode structure as shown in Fig. 14^[81]. It is quite obvious from the figure that H₂ and H₂O have opposite fluxes within the anode, because the former is being consumed and the latter is being produced as a result of electrochemical reactions at the three-phase interface. The computed temperature distribution in a single planer cell operated with humidified methane (97% CH₄ and 3% H₂O) as fuel at adiabatic conditions and assuming H₂ as the only electrochemically active species, the local variation of temperature in the fuel and air channels as well as in the interconnects are shown in Fig. 15^[82]. At the entrance, the fuel stream loses heat to the comparatively cold air entering the air channel, hence the temperature of the air stream increases. As reforming starts, the temperature of the fuel stream further drops and now, the temperature of the air stream as well. However, further downstream, the temperature begins to increase as a result of exothermic thermo catalytic cell reactions such as water-gas shift, electrochemical oxidation as well as ohmic and activation losses. There is no significant temperature difference between the anode side interconnect and the fuel channel in contrast to the behavior at the cathode side interconnect/air channel. Interestingly, the temperature of the anode side interconnect is lower than that of the fuel channel, while the cathode side interconnect has a higher temperature than the air channel, which is primarily caused by thermal radiation from the cathode electrode to the interconnect.

This model approach was also used to study the influence of air flow rate, anode thickness, catalyst loading, and pre-reforming on the performance of a planar anode-supported cell, which was 10 cm in length and operated with 40% CH₄ and 60% H₂O as fuel at 0.7 V. Since the cell voltage was fixed, fuel utilization is the most significant parameter for cell efficiency. For any particular operating condition, an optimal anode thickness exists for efficiency and power density (Fig. 16)^[83]; maxima were achieved for an anode thickness of approximately 0.5 mm under the

conditions of this study. In the case of direct internal fuel reforming, the anode serves as catalyst for the production of H₂ and CO that further participate in the charge transfer reactions at the three-phase boundary. In the case of thin anodes, the smaller amount of catalyst limits the amount of H₂ produced leading to lower average current density, efficiency, and power density. For thick anodes, the H₂ and CO production by the (endothermic) fuel reforming is increased, however, on the costs of a larger temperature drop close to channel inlet resulting in decreased performance.

Acknowledgment

The author would like to thank J. Warnatz (University of Heidelberg), L.D. Schmidt (University of Minnesota), and R.J. Kee (Colorado School of Mines) for fruitful collaborations and stimulating discussions.

References

- [1] D. A. Hickman, L. D. Schmidt, *Journal of Catalysis* **1992**, 138, 267.
- [2] O. Deutschmann, L. D. Schmidt, *American Institute of Chemical Engineering Journal* **1998**, 44, 2465.
- [3] M. C. Huff, L. D. Schmidt, *Journal of Catalysis* **1993**, 149, 127.
- [4] D. K. Zerkle, M. D. Allendorf, M. Wolf, O. Deutschmann, *Journal of Catalysis* **2000**, 196, 18.
- [5] H. Y. Zhu, R. J. Kee, V. M. Janardhanan, O. Deutschmann, D. G. Goodwin, *Journal of the Electrochemical Society* **2005**, 152, A2427.
- [6] E. S. Hecht, G. K. Gupta, H. Y. Zhu, A. M. Dean, R. J. Kee, L. Maier, O. Deutschmann, *Applied Catalysis a-General* **2005**, 295, 40.
- [7] J. Windmann, J. Braun, P. Zacke, S. Tischer, O. Deutschmann, J. Warnatz, *SAE Technical Paper* **2003**, 2003-01-0937.
- [8] R. B. Bird, W. E. Stewart, E. N. Lightfoot, *Transport Phenomena*, 2nd ed., John Wiley & Sons, Inc., New York, **2001**.
- [9] S. V. Patankar, *Numerical Heat Transfer and Fluid Flow*, McGraw-Hill, New York, **1980**.
- [10] J. Warnatz, R. W. Dibble, U. Maas, *Combustion, Physical and Chemical Fundamentals, Modeling and Simulation, Experiments, Pollutant Formation*, Springer-Verlag, New York, **1996**.
- [11] R. E. Hayes, S. T. Kolaczkowski, *Introduction to Catalytic Combustion*, Gordon and Breach Science Publ., Amsterdam, **1997**.
- [12] R. J. Kee, M. E. Coltrin, P. Glarborg, *Chemically Reacting Flow*, Wiley-Interscience, **2003**.
- [13] O. Deutschmann, in *Handbook of Heterogeneous Catalysis*, 2nd Ed. (Ed.: H. K. G. Ertl, F. Schüth, J. Weitkamp), Wiley-VCH, **2007**.
- [14] E. Ranzi, A. Sogaro, P. Gaffuri, G. Pennati, C. K. Westbrook, W. J. Pitz, *Combustion and Flame* **1994**, 99, 201.
- [15] M. E. Coltrin, R. J. Kee, F. M. Rupley, *SURFACE CHEMKIN (Version 4.0): A Fortran Package for Analyzing Heterogeneous Chemical Kinetics at a Solid-Surface - Gas-Phase Interface*, SAND91-8003B, Sandia National Laboratories, **1991**.
- [16] A. B. Mhadeshwar, H. Wang, D. G. Vlachos, *Journal of Physical Chemistry B* **2003**, 107, 12721.
- [17] W. R. Williams, C. M. Marks, L. D. Schmidt, *Journal of Physical Chemistry* **1992**, 96, 5922.
- [18] B. Hellsing, B. Kasemo, V. P. Zhdanov, *Journal of Catalysis* **1991**, 132, 210.
- [19] J. Warnatz, *Proceedings of the Combustion Institute* **1992**, 24, 553.
- [20] M. Rinnemo, O. Deutschmann, F. Behrendt, B. Kasemo, *Combustion and Flame* **1997**, 111, 312.
- [21] G. Veser, *Chemical Engineering Science* **2001**, 56, 1265.
- [22] P.-A. Bui, D. G. Vlachos, P. R. Westmoreland, *Industrial & Engineering Chemistry Research* **1997**, 36, 2558.
- [23] J. C. G. Andrae, P. H. Björnbohm, *American Institute of Chemical Engineering Journal* **2000**, 46, 1454.
- [24] J. Mai, W. von Niessen, A. Blumen, *Journal of Chemical Physics* **1990**, 93, 3685.
- [25] V. P. Zhdanov, B. Kasemo, *Applied Surface Science* **1994**, 74, 147.
- [26] P. Aghalayam, Y. K. Park, D. G. Vlachos, *Proceedings of the Combustion Institute* **2000**, 28, 1331.
- [27] O. Deutschmann, R. Schmidt, F. Behrendt, J. Warnatz, *Proceedings of the Combustion Institute* **1996**, 26, 1747.
- [28] G. Veser, J. Frauhammer, L. D. Schmidt, G. Eigenberger, in *Studies in Surface Science and Catalysis 109*, **1997**, pp. 273.
- [29] P.-A. Bui, D. G. Vlachos, P. R. Westmoreland, *Surface Science* **1997**, 386, L1029.

- [30] U. Dogwiler, P. Benz, J. Mantzaras, *Combustion and Flame* **1999**, *116*, 243.
- [31] P. Aghalayam, Y. K. Park, N. Fernandes, V. Papavassiliou, A. B. Mhadeshwar, D. G. Vlachos, *Journal of Catalysis* **2003**, *213*, 23.
- [32] D. A. Hickman, L. D. Schmidt, *American Institute of Chemical Engineering Journal* **1993**, *39*, 1164.
- [33] M. Huff, L. D. Schmidt, *Journal of Physical Chemistry* **1993**, *97*, 11815.
- [34] M. C. Huff, I. P. Androulakis, J. H. Sinfelt, S. C. Reyes, *Journal of Catalysis* **2000**, *191*, 46.
- [35] F. Donsi, K. A. Williams, L. D. Schmidt, *Industrial & Engineering Chemistry Research* **2005**, *44*, 3453.
- [36] R. Schwiedernoch, S. Tischer, C. Correa, O. Deutschmann, *Chemical Engineering Science* **2003**, *58*, 633.
- [37] D. Chatterjee, O. Deutschmann, J. Warnatz, *Faraday Discussions* **2001**, *119*, 371.
- [38] B. Ruf, F. Behrendt, O. Deutschmann, J. Warnatz, *Surface Science* **1996**, *352*, 602.
- [39] S. J. Harris, D. G. Goodwin, *Journal of Physical Chemistry* **1993**, *97*, 23.
- [40] S. Romet, M. F. Couturier, T. K. Whidden, *Journal of the Electrochemical Society* **2001**, *148*, G82.
- [41] C. D. Scott, A. Povitsky, C. Dateo, T. Gokcen, P. A. Willis, R. E. Smalley, *Journal of Nanoscience and Nanotechnology* **2003**, *3*, 63.
- [42] A. Beretta, P. Forzatti, E. Ranzi, *Journal of Catalysis* **1999**, *184*, 469.
- [43] A. Beretta, P. Forzatti, *Journal of Catalysis* **2001**, *200*, 45.
- [44] A. Beretta, E. Ranzi, P. Forzatti, *Chemical Engineering Science* **2001**, *56*, 779.
- [45] R. Subramanian, L. D. Schmidt, *Angewandte Chemie-International Edition* **2005**, *44*, 302.
- [46] J. J. Krummenacher, L. D. Schmidt, *Journal of Catalysis* **2004**, *222*, 429.
- [47] L. D. Schmidt, J. Siddall, M. Bearden, *American Institute of Chemical Engineering Journal* **2000**, *46*, 1492.
- [48] L. L. Raja, R. J. Kee, L. R. Petzold, *Proceedings of the Combustion Institute* **1998**, *27*, 2249.
- [49] D. Papadias, L. Edsberg, P. H. Björnbohm, *Catalysis Today* **2000**, *60*, 11.
- [50] F. Keil, *Diffusion und Chemische Reaktionen in der Gas-Feststoff-Katalyse*, Springer-Verlag, Berlin, **1999**.
- [51] F. J. Keil, *Catalysis Today* **2000**, *53*, 245.
- [52] U. Maas, S. Pope, *Combustion and Flame* **1992**, *88*, 239.
- [53] X. Yan, U. Maas, *Proceedings of the Combustion Institute* **2000**, *28*, 1615.
- [54] R. G. Susnow, A. M. Dean, W. H. Green, P. Peczak, L. Broadbelt, *Journal of Physical Chemistry A* **1997**, *101*, 3731.
- [55] S. Tischer, C. Correa, O. Deutschmann, *Catalysis Today* **2001**, *69*, 57.
- [56] S. Tischer, O. Deutschmann, *Catalysis Today* **2005**, *105*, 407.
- [57] O. Deutschmann, S. Tischer, C. Correa, D. Chatterjee, S. Kleditzsch, V. M. Janardhanan, *DETCHEM software package*, 2.0 ed., www.detchem.com, Karlsruhe, **2004**.
- [58] C. Appel, J. Mantzaras, R. Schaeren, R. Bombach, A. Inauen, *Combustion and Flame* **2005**, *140*, 70.
- [59] H. P. A. Calis, J. Nijenhuis, B. C. Paikert, F. M. Dautzenberg, C. M. van den Bleek, *Chemical Engineering Science* **2001**, *56*, 1713.
- [60] C. Appel, J. Mantzaras, R. Schaeren, R. Bombach, B. Kaeppli, A. Inauen, *Proceedings of the Combustion Institute* **2002**, *29*, 1031.
- [61] C. Appel, J. Mantzaras, R. Schaeren, R. Bombach, A. Inauen, B. Kaeppli, B. Hemmerling, A. Stampanoni, *Combustion and Flame* **2002**, *128*, 340.
- [62] H. D. Minh, H. G. Bock, S. Tischer, O. Deutschmann, *Aiche Journal* **2008**, *54*, 2432.
- [63] H. D. Minh, H. G. Bock, S. Tischer, O. Deutschmann, *Computational Science and Its Applications - Iccsa 2008, Pt 1, Proceedings* **2008**, *5072*, 1121.
- [64] M. von Schwerin, O. Deutschmann, V. Schulz, *Computers & Chemical Engineering* **2000**, *24*, 89.
- [65] J. Mantzaras, C. Appel, P. Benz, U. Dogwiler, *Catalysis Today* **2000**, *59*, 3.
- [66] C. Appel, J. Mantzaras, R. Schaeren, R. Bombach, B. Kaeppli, A. Inauen, *Proceedings of the Combustion Institute* **2003**, *29*, 1031.
- [67] L. D. Schmidt, O. Deutschmann, C. T. Goralski, in *Natural Gas Conversion V, Vol. 119*, **1998**, pp. 685.
- [68] R. Horn, K. A. Williams, N. J. Degenstein, L. D. Schmidt, *Journal of Catalysis* **2006**, *242*, 92.
- [69] R. Quiceno, J. Perez-Ramirez, J. Warnatz, O. Deutschmann, *Applied Catalysis a-General* **2006**, *303*, 166.
- [70] B. T. Schadel, M. Duisberg, O. Deutschmann, *Catalysis Today* **2009**, *142*, 42.
- [71] M. C. Huff, L. D. Schmidt, *Journal of Physical Chemistry* **1993**, *97*, 11815.
- [72] A. S. Bodke, D. A. Olschki, L. D. Schmidt, E. Ranzi, *Science* **1999**, *285*, 712.
- [73] D. K. Zerkle, M. D. Allendorf, M. Wolf, O. Deutschmann, *Proceedings of the Combustion Institute* **2000**, *28*, 1365.
- [74] J. J. Krummenacher, K. N. West, L. D. Schmidt, *Journal of Catalysis* **2003**, *215*, 332.
- [75] E. C. Wanat, K. Venkataraman, L. D. Schmidt, *Applied Catalysis a-General* **2004**, *276*, 155.
- [76] G. A. Deluga, J. R. Salge, L. D. Schmidt, X. E. Verykios, *Science* **2004**, *303*, 993.
- [77] M. Hartmann, L. Maier, O. Deutschmann, *Combustion and Flame* **2010**, *157*, 1771.
- [78] S. Park, J. M. Vohs, R. J. Gorte, *Nature (London)* **2000**, *404*, 265.

- [79] V.M. Janardhanan, O. Deutschmann, *Journal of Power Sources* **2006**, 162, 1192.
- [80] H. Zhu, R. J. Kee, *Journal of Power Sources* **2003**, 117, 61.
- [81] V. M. Janardhanan, O. Deutschmann, *Zeitschrift Fur Physikalische Chemie-International Journal of Research in Physical Chemistry & Chemical Physics* **2007**, 221, 443.
- [82] V. M. Janardhanan, O. Deutschmann, *Chemical Engineering Science* **2007**, 62, 5473.
- [83] V. M. Janardhanan, V. Heuveline, O. Deutschmann, *Journal of Power Sources* **2007**, 172, 296.

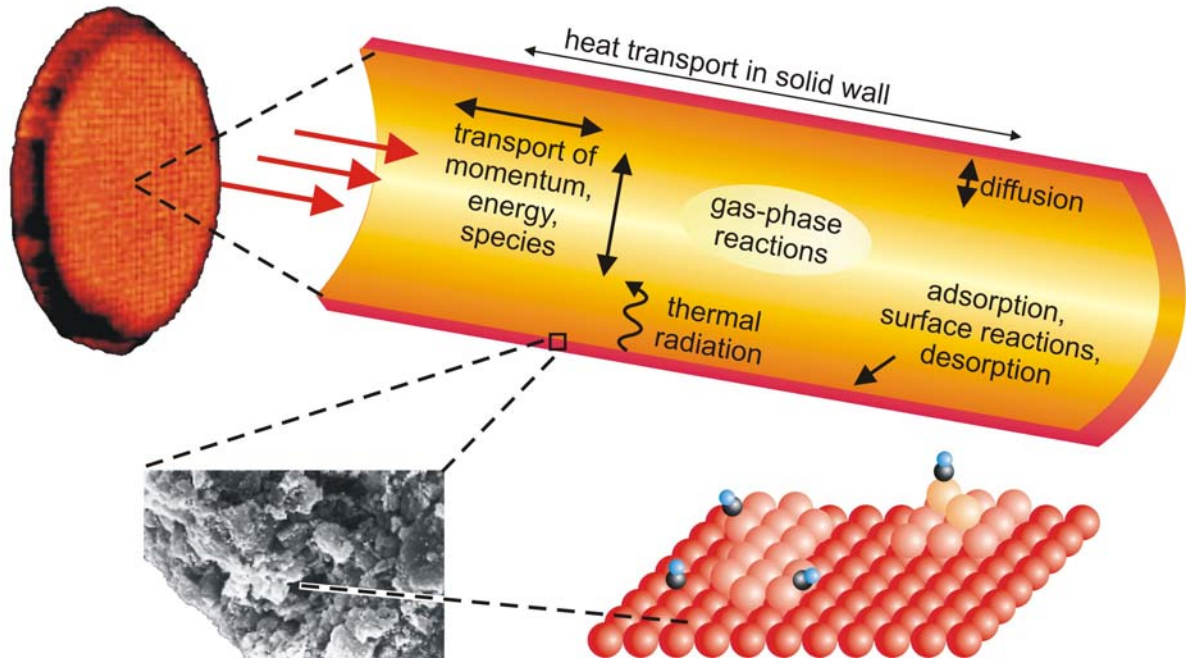


Fig. 1: Catalytic combustion monolith and physical and chemical process occurring in the single monolith channel.

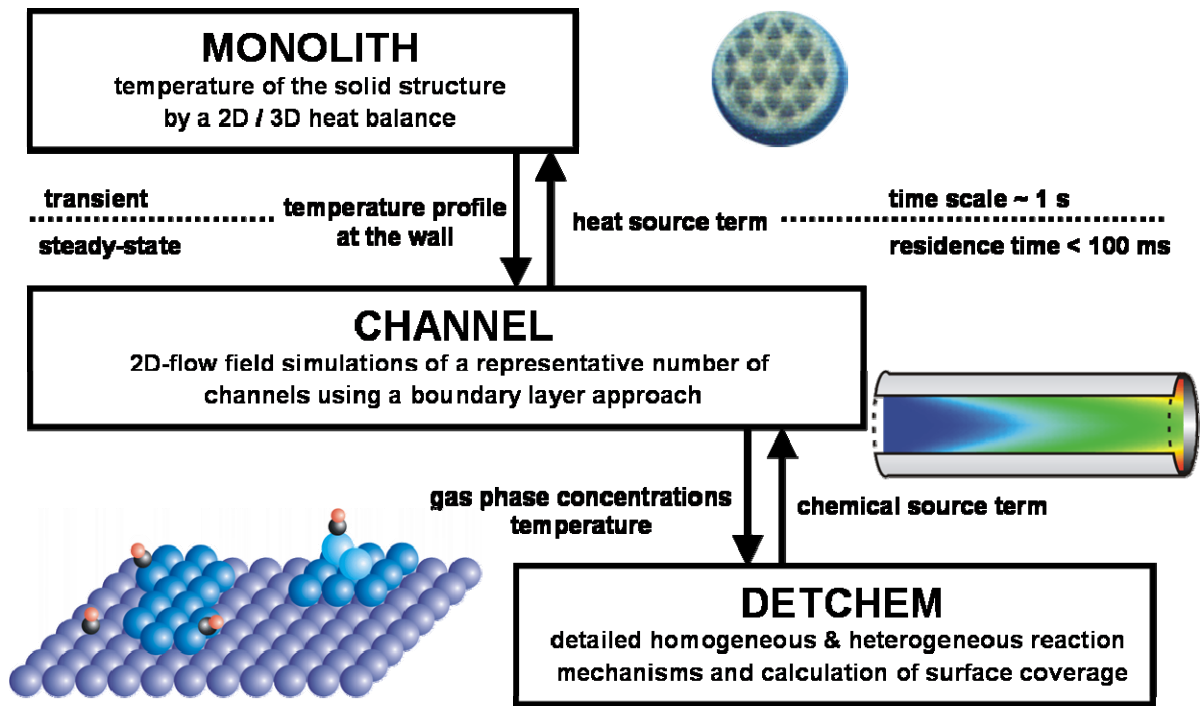


Fig. 2: Structure of the code DETCHEM^{MONOLITH} [57].

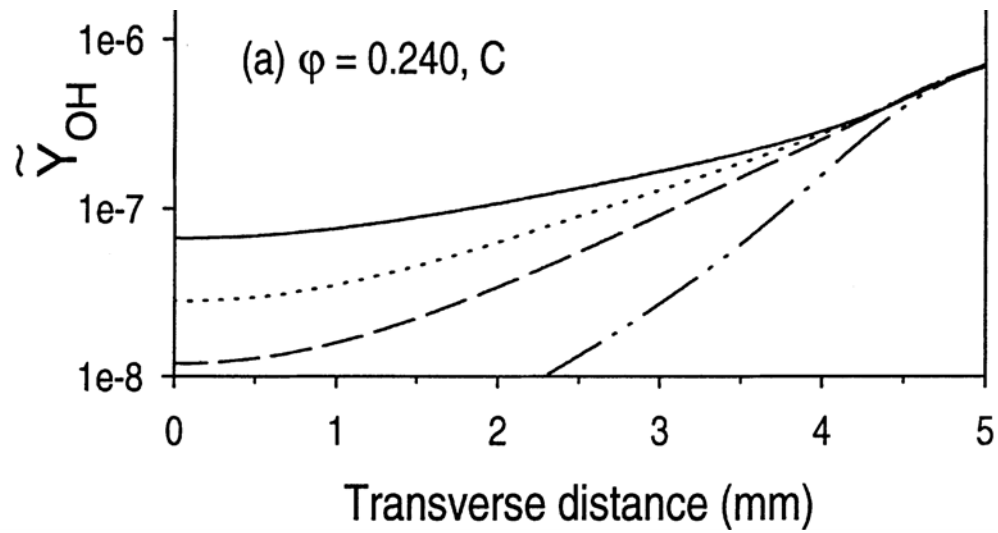


Fig. 3: Transverse profiles of normalized Favre-averaged OH mass fractions in catalytically supported oxidation of hydrogen over a platinum wall. Streamwise distances: $x=25\text{mm}$ (dash-double dotted), $x=61\text{mm}$ (dashed), $x=98\text{mm}$ (dotted), and $x=150\text{mm}$ (solid) lines. The wall is located at $y=5\text{ mm}$ taken from Mantzaras et al.^[65].

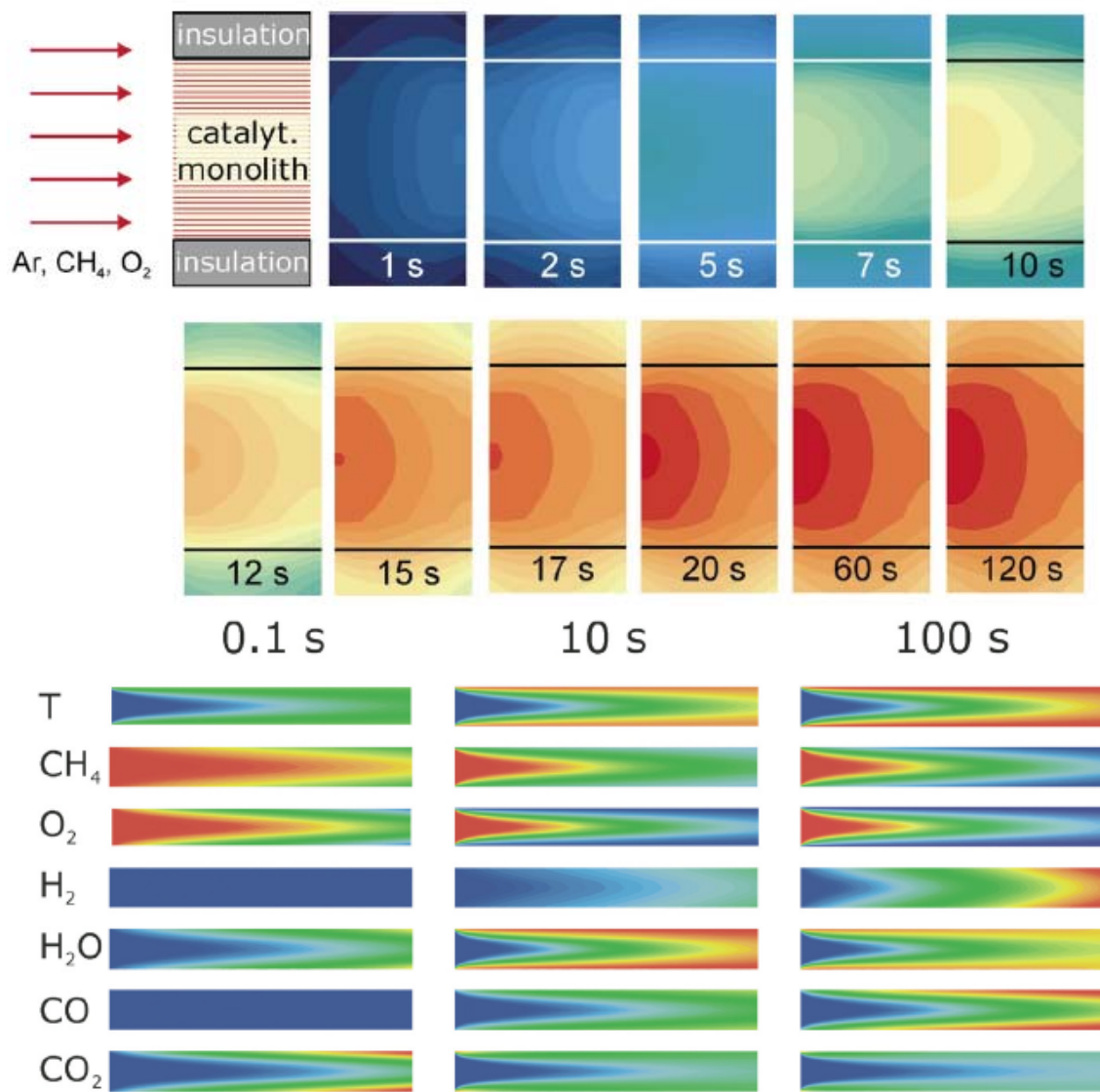


Fig. 4: Simulation of light-off of a monolithic reactor coated with Rh for partial oxidation of methane to synthesis gas ^[36]. Temperature of the solid structure (top) and gas-phase temperature and species mole fractions in a single channel in the center of the monolith (below), red = maximum, blue = minimum.

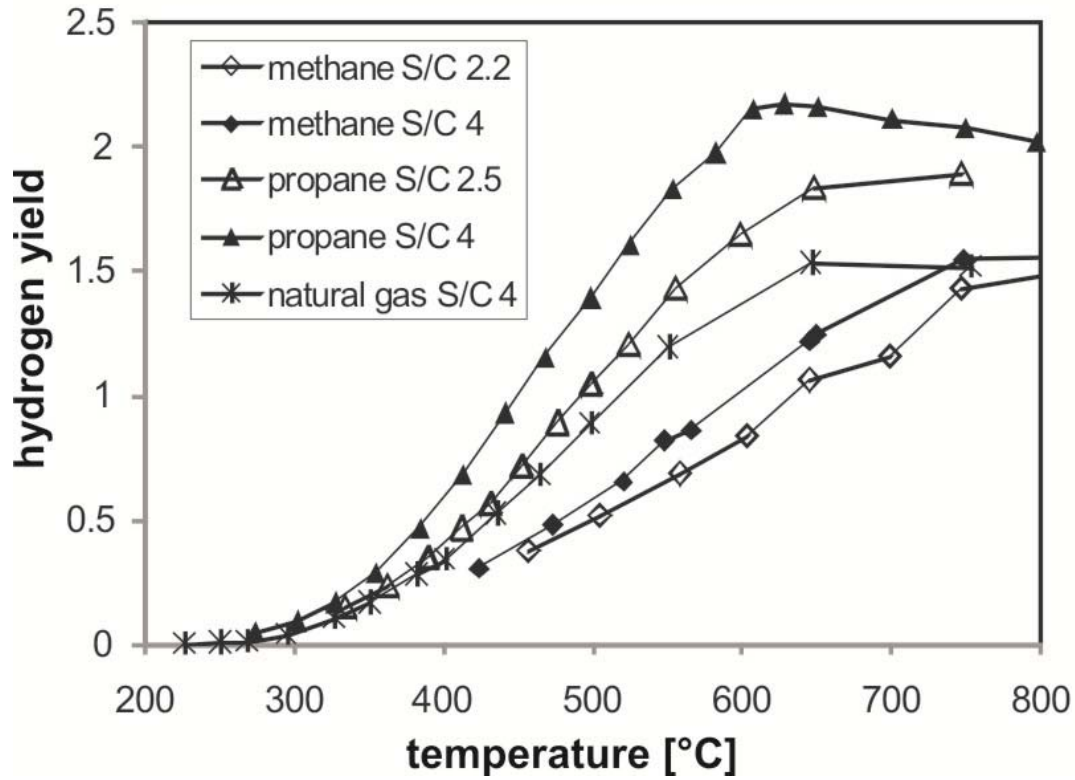


Fig. 5: Comparison of experimentally determined hydrogen yields in steam-reforming of methane with S/C 2.5 (◇) and S/C 4 (◆), steam reforming of natural gas with S/C 4 (*), steam reforming of propane with S/C 2.5 (△) and S/C 4 (▲); Rh catalyst, taken from^[70].

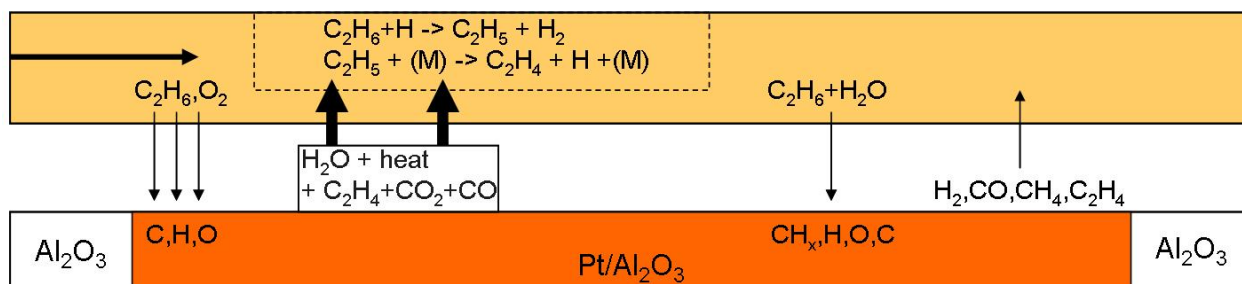


Fig. 6: General picture of oxy-dehydrogenation of ethane over Pt at millisecond contact times and temperatures of $\sim 900^\circ\text{C}$; inlet ethane/oxygen ratio ~ 2 . The upper and lower panel show gas-phase and surface processes, respectively, adapted from Zerkle et al.^[4].

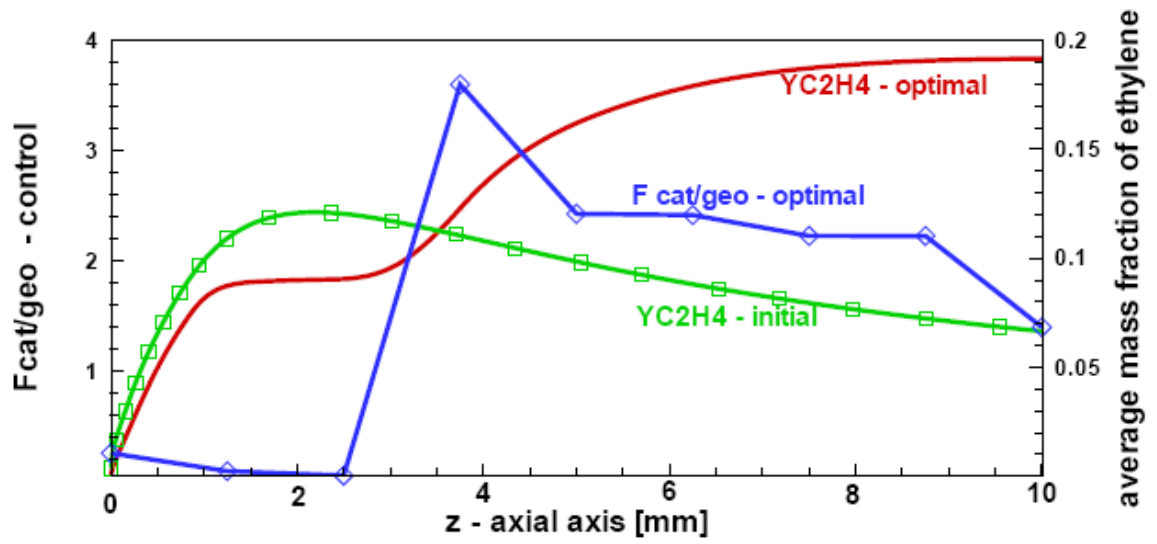


Fig. 7: Catalyst loading expressed by $F_{\text{cat/geo}}(z)$ and the radial averaged mass fraction of ethylene at the initial and at optimal solutions in oxy-dehydrogenation of ethane over Pt coated honeycomb monoliths, taken from Minh et al.^[62].

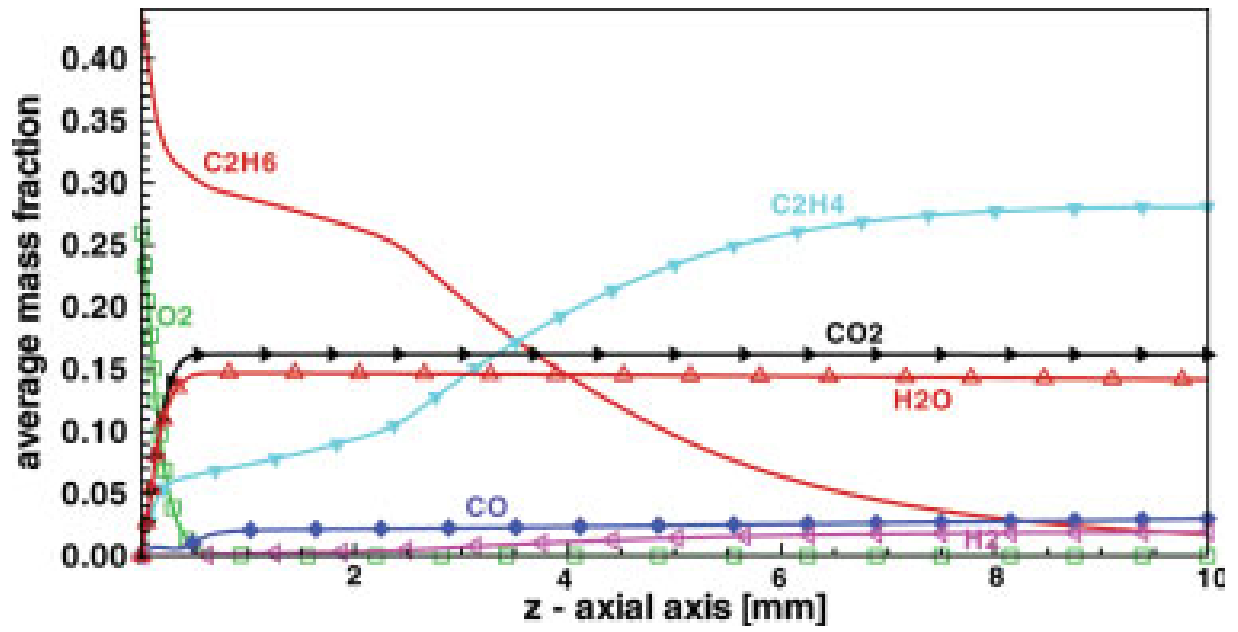


Fig. 8: Average mass fractions of major species at the optimal solution in optimization of catalyst loading in oxy-dehydrogenation of ethane over Pt coated honeycomb monoliths, taken from Minh et al.^[62].

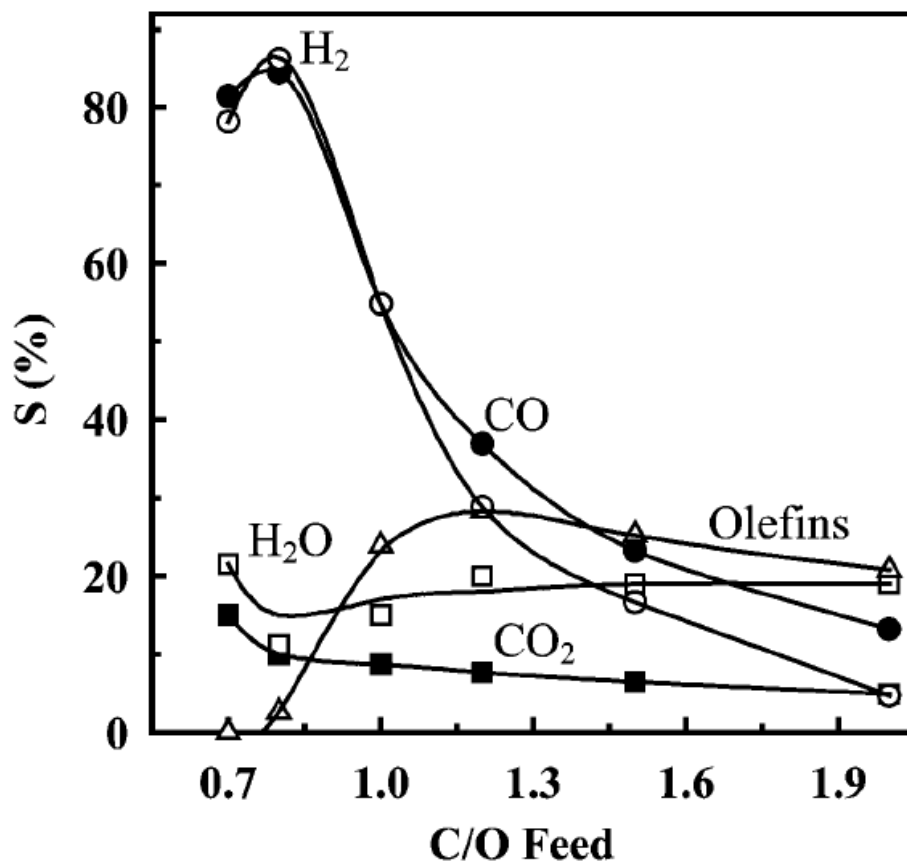


Fig. 9: Effect of the n-decane/oxygen feed ratio on the product selectivity in CPOX of n-decane at millisecond contact times over Rh catalysts^[46].

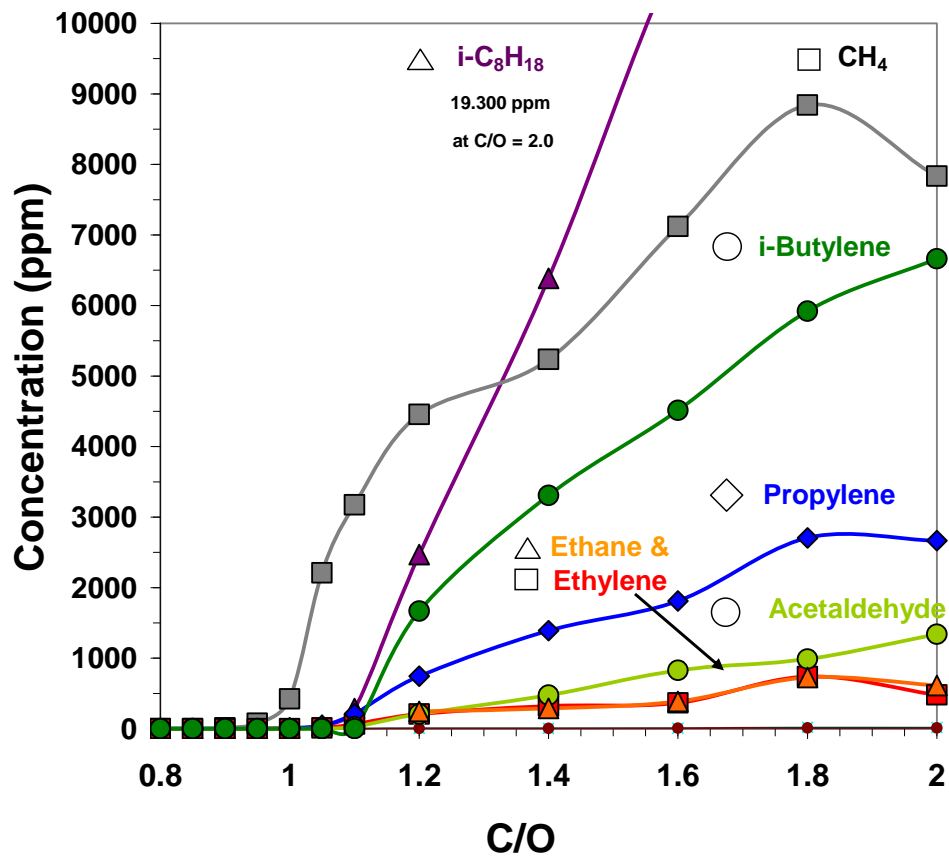


Fig. 10: Experimentally determined concentrations of the side products and the fuel remaining in the outlet stream of CPOX of *i*-octane over a Rh/alumina coated monolith as a function of C/O ratio, taken from^[77].

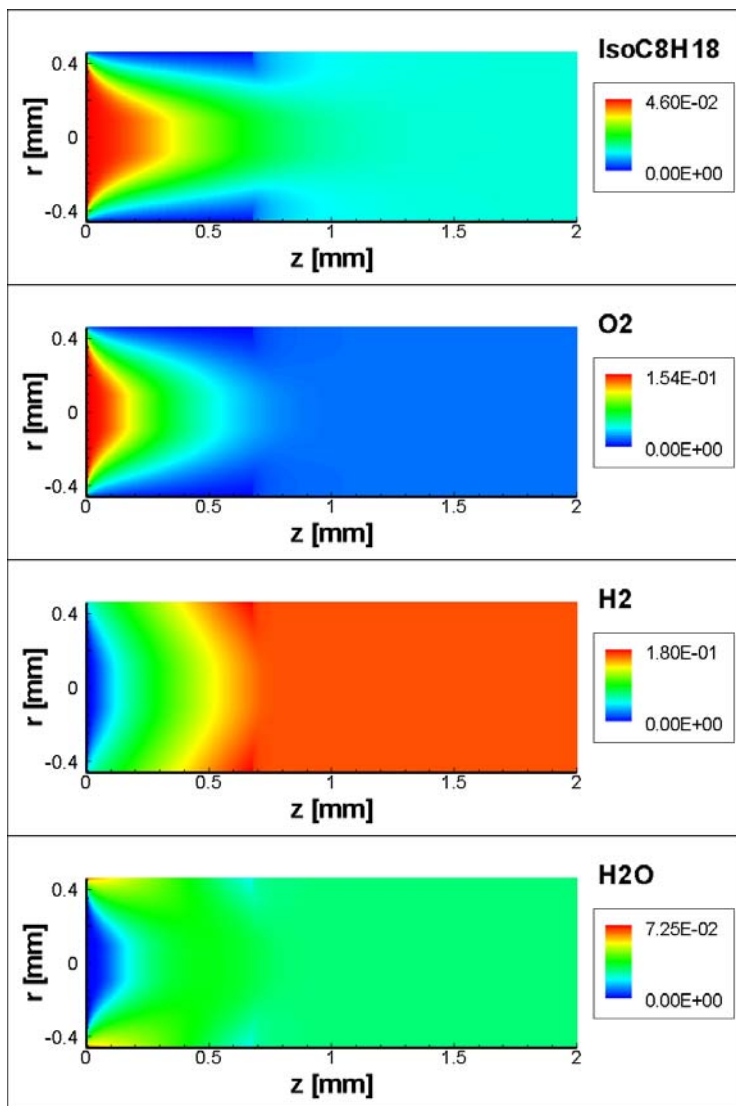


Fig. 11: Numerically predicted profiles of molar fractions of reactants and major products in the entrance region of the catalyst at $C/O=1.2$ in CPOX of iso-octane over a Rh/alumina coated monolith, taken from Hartmann et al.^[77]. Flow direction is from left to right.

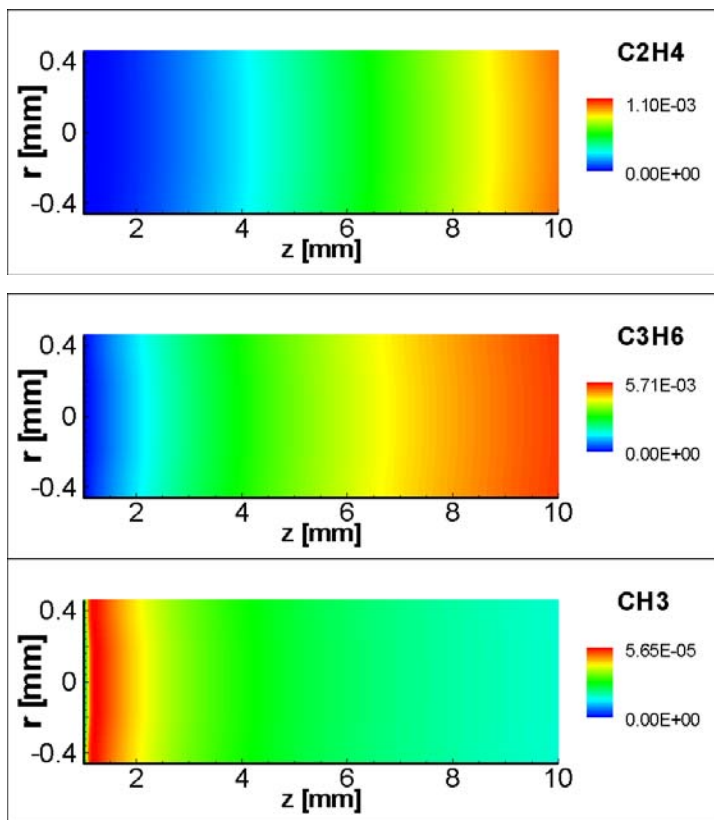


Fig. 12: Numerically predicted profiles of molar fractions of minor products and radicals along the entire catalyst at $C/O=1.2$ in CPOX of iso-octane over a Rh/alumina coated monolith, taken from Hartmann et al.^[77]. Flow direction is from left to right.

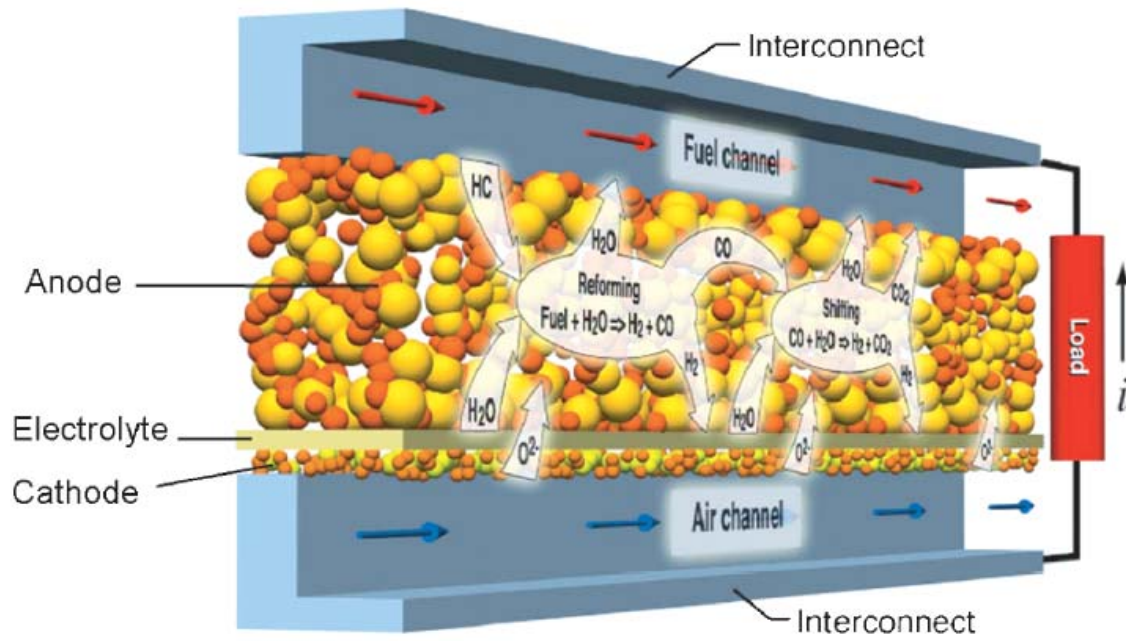


Fig. 13: A schematic presentation of a cut-away view of a planar, anode-supported SOFC unit in co-flow configuration operated with hydrocarbon containing fuels; adapted from Zhu et al.^[5].

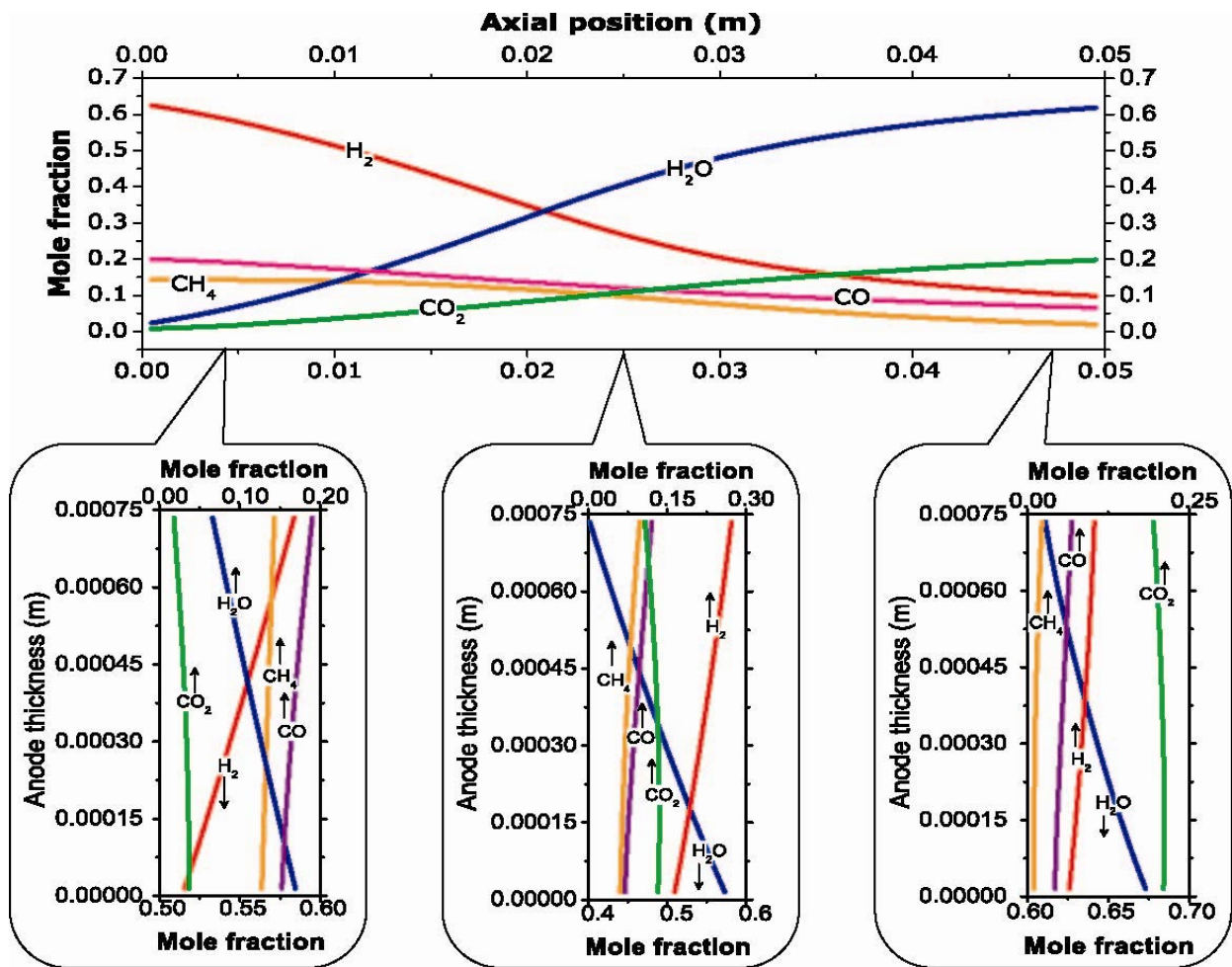


Fig. 14: Numerically predicted species profiles within the fuel channel and within the anode of a SOFC. The inlet fuel at 800°C is assumed to consist of 14% CH₄, 63% H₂, 2% H₂O, 20% CO, and traces of CO₂. Air is assumed to enter the cathode channel at 650°C. The drop down panels shows the profiles across the thickness of the anode at selected axial positions.

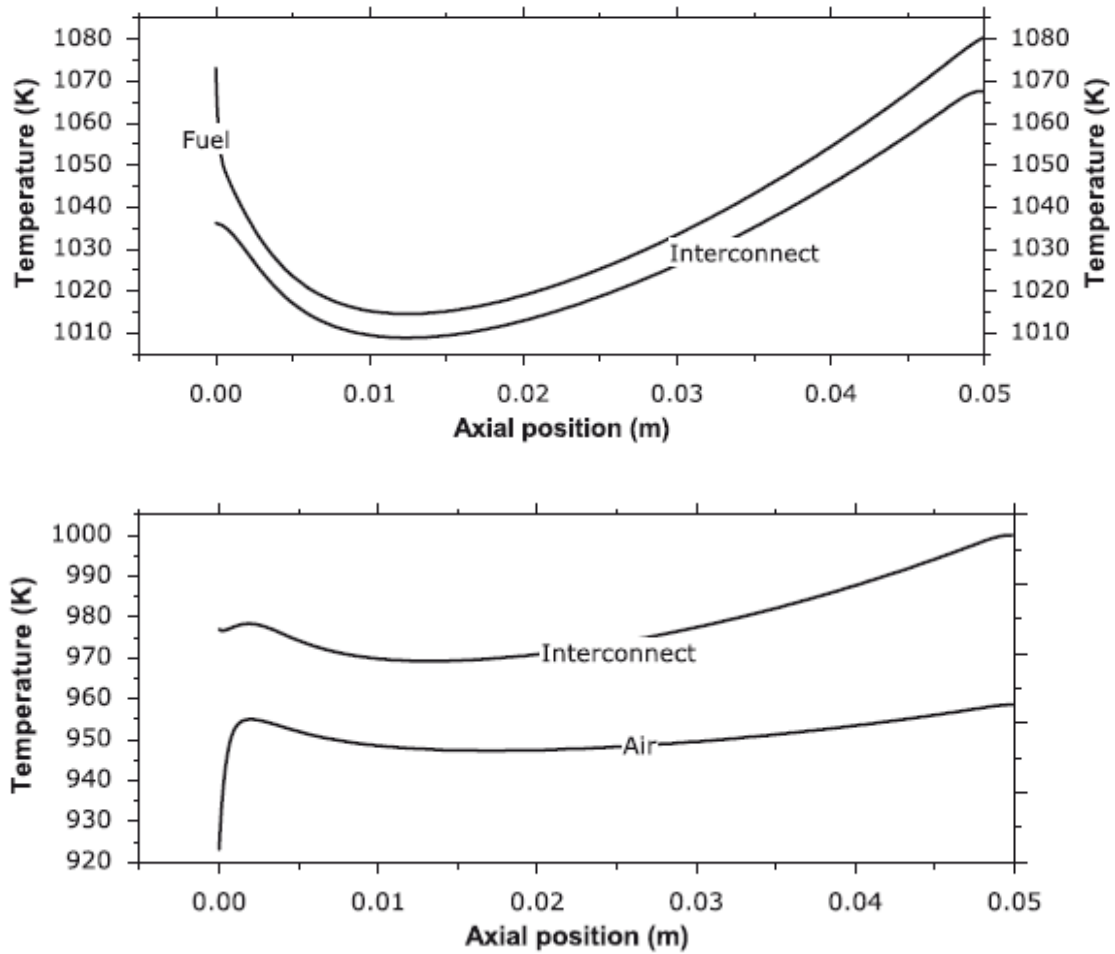


Fig. 15: Numerical predictions of temperature profiles within the flow (top) and air (bottom) channels as well as in the interconnects in a SOFC cell operated with humidified methane as fuel. The inlet fuel and air streams are at 800 °C and 650 °C, respectively; operating cell potential is 0.7V, taken from^[82].

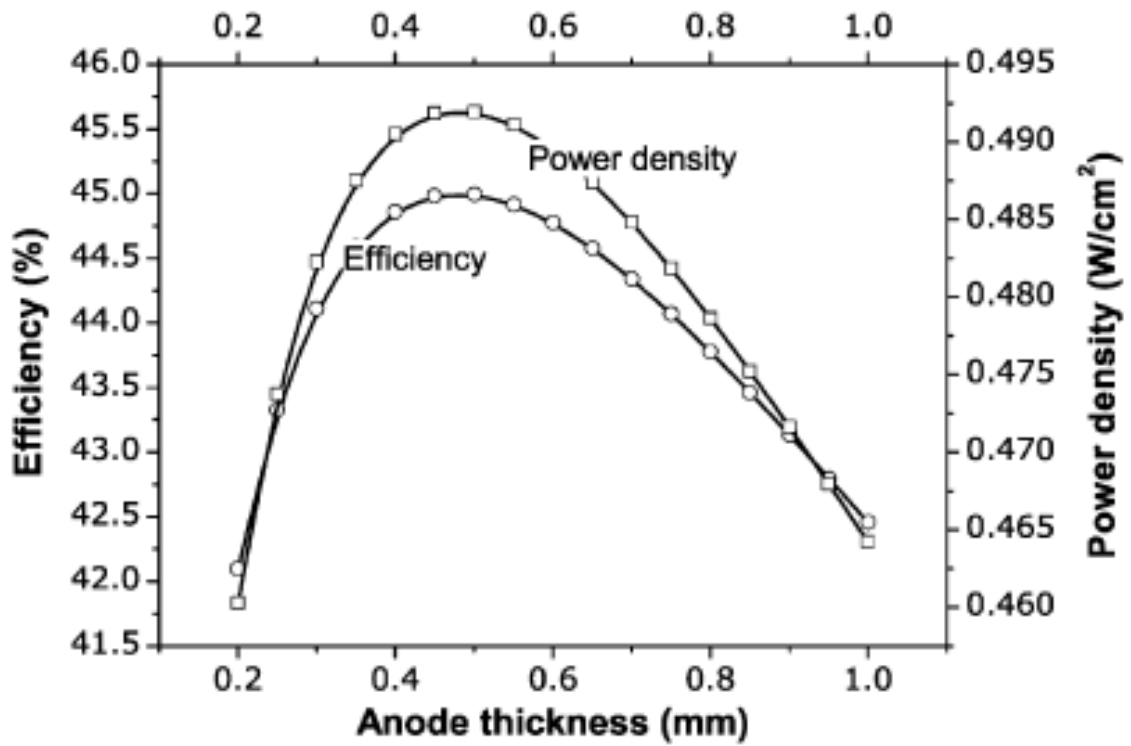


Fig. 16: Effect of anode thickness on efficiency and power density for a cell operated under adiabatic conditions. The inlet fuel consists of 40% CH₄ and 60% H₂O at 800°C. Cathode inlet is assumed to be air at 650°C. Figure taken from Janardhanan et al. [83].